



1 **Construction and Application of a Pollen Emissions Model**
2 **based on Phenology and Random Forests**

3 Jiangtao Li^{a,b}, Xingqin An^{a,*}, Zhaobin Sun^a, Caihua Ye^c, Qing Hou^a, Yuxin Zhao^a, Zhe
4 Liu^a

5 ^a State Key Laboratory of Severe Weather, Chinese Academy of Meteorological
6 Sciences, Beijing, 100081, China

7 ^b Department of Atmospheric and Oceanic Sciences & Institute of Atmospheric
8 Sciences, Fudan University, Shanghai, 200438, China

9 ^c Meteorological Service Center of Beijing Meteorological Bureau, Beijing, 100089,
10 China

11 * Corresponding author: Xingqin An

12 Email address: anxq@cma.gov.cn

13 **Abstract:** In recent years, the intensification of global climate change and
14 environmental pollution has led to a marked increase in pollen-induced allergic
15 diseases. This study leverages 16 years of continuous pollen monitoring data,
16 alongside meteorological factors and plant functional type data, to construct a pollen
17 emissions model using phenology and random forests (RF). This model is then
18 employed to simulate the emission characteristics of three primary types of autumn
19 pollen (Artemisia, Chenopod, and total pollen concentration), elucidating the emission
20 patterns throughout the seasonal cycle in Beijing. Phenology and RF precisely
21 simulate the start and end day of year of pollen, as well as the annual pollen
22 production. There are significant spatiotemporal differences among the three types of
23 pollen. On average, pollen dispersal begins around August 10, peaks around August
24 30, and concludes by September 25, with a dispersal period lasting approximately 45
25 days. Furthermore, the relationship between pollen emissions and meteorological
26 factors is investigated, revealing that temperature, relative humidity (RH), and
27 sunshine hours (SSH) significantly influence annual pollen emissions. Specifically,
28 temperature and RH exhibit a strong positive correlation with annual pollen emissions,



29 while SSH shows a negative correlation. Different pollen types display varied
30 responses to meteorological factors. Finally, the constructed pollen emissions model is
31 integrated into RegCM and validated using pollen observation data, confirming its
32 reliability in predicting pollen concentrations. This study not only enhances the
33 understanding of pollen release mechanisms but also provides scientific evidence for
34 the selection and planting of urban greening plants.

35 **Keywords:** Pollen Emissions Model, Phenology, Random Forests, RegCM

36 1. Introduction

37 Pollen are microscopic particles, typically ranging from 5 to 100 micrometers in
38 diameter, released by plants to transfer male genetic material for reproduction. These
39 particles, significant allergens, disperse into the atmosphere via wind, contributing to
40 atmospheric particulate matter, interacting with clouds and radiation, and playing a
41 pivotal role in plant fertilization and gene dissemination (Damialis et al., 2011; Lei et
42 al., 2023). Additionally, pollen is linked to allergic diseases such as allergic rhinitis
43 and asthma and may even elevate the risk of gastrointestinal and neurological
44 disorders (Guzman et al., 2007; Krishna et al., 2020; Chen et al., 2021; Stas et al.,
45 2021). In China, the incidence of pollen allergies has surged from 5 % to 17.8 % and
46 continues to rise rapidly (Lou et al., 2017). Pollen-induced respiratory allergic
47 symptoms, such as allergic rhinitis (AR), affect up to 30 % of the global population,
48 particularly children under 18 (Mir et al., 2012; Wang et al., 2016; Zhang and Steiner,
49 2022; Zhao et al., 2023). It is generally believed that these respiratory allergic
50 diseases are more prevalent in developed countries (Emanuel, 1988; Ibrahim et al.,
51 2021). However, the International Study of Asthma and Allergies in Childhood
52 (ISAAC) global reports indicate that these diseases are equally or even more prevalent
53 in some developing countries compared to developed ones (Asher et al., 2006; Mallol
54 et al., 2013). Children, as a vulnerable population, are particularly susceptible to AR
55 and its complications (Cingi et al., 2017). Without effective early intervention, allergic
56 symptoms in children can persist throughout their lives, imposing a substantial
57 economic burden on families and healthcare systems (Ahmed et al., 2018) and



58 potentially posing a life-threatening risk (Schmidt, 2016). In China, a densely
59 populated developing country, the proportion of pediatric allergic diseases within the
60 spectrum of childhood illnesses is increasing annually, leading to significant
61 economic and health losses due to medical expenses, impacts on human life, and
62 premature death. Furthermore, since pollen release is closely linked to environmental
63 factors, climate change may influence pollen release, thereby affecting the incidence
64 of allergic diseases (Wang et al., 2018; Bishan et al., 2020). In recent decades, the
65 pollen season has exhibited a trend of becoming longer and more intense, which may
66 exacerbate the conditions of allergic rhinitis and asthma (D'Amato et al., 2016; Lake
67 et al., 2017a; Aerts et al., 2020; Kurganskiy et al., 2021)..

68 With the improvement in living standards and heightened health awareness,
69 airborne pollen diseases, such as hay fever, have garnered widespread attention. As a
70 typical seasonal epidemic (Yin et al., 2005; Lei et al., 2023), hay fever significantly
71 impacts global health. Existing studies have demonstrated that the incidence of
72 airborne pollen diseases is closely associated with the concentration of airborne
73 allergenic pollen, particularly during peak pollen seasons (Frei and Gassner, 2008;
74 Bastl et al., 2018; Kurganskiy et al., 2021). Due to the regional nature of airborne
75 pollen, the types and concentrations of pollen vary geographically. Although the
76 annual variation trend of total pollen amount generally exhibits a similar bimodal
77 pattern, increasing annual climatic variability amidst global warming has led to
78 significant changes in the pollen seasons of various plants, with discrepancies of more
79 than 20 days in some years. This variability poses practical challenges for conducting
80 pollen monitoring research and providing public meteorological services (He et al.,
81 2001; Gu and Liao, 2003; Bai et al., 2009; Lei et al., 2023). Therefore, studying
82 pollen concentration and distribution is crucial for understanding the pathogenesis of
83 airborne pollen diseases, conducting effective pollen monitoring research, and
84 delivering accurate public meteorological services.

85 However, compared to regions such as Europe and the United States, China faces
86 significant challenges in pollen monitoring due to fewer monitoring stations, shorter
87 monitoring histories, and a lower prevalence of automated facilities. These limitations



88 have resulted in China's pollen simulation research remaining primarily at the level of
89 simple statistical methods, focusing only on basic statistical studies of the impact of
90 meteorological conditions on pollen concentration. In contrast, numerical models are
91 rarely employed for regional simulation of pollen concentration. This situation
92 reflects the relative lag in China's pollen monitoring and research system, hindering a
93 deeper understanding of pollen dispersion patterns and the scientific study of related
94 health issues (Wu et al., 2011; Meng et al., 2016; Guan et al., 2021; Gao et al., 2022).

95 Although numerical models play a crucial role in simulating pollen concentration,
96 they require a clear understanding of pollen emissions. Pollen emissions are
97 influenced not only by meteorological factors but also by vegetation types, land use
98 changes, and human activities (Sofiev et al., 2006; Wozniak and Steiner, 2017; Zhang
99 and Steiner, 2022; He et al., 2023; Lei et al., 2023). Particularly in the context of
100 accelerated urbanization, the selection and layout of urban greening plants have a
101 significant impact on pollen emissions. The complex interactions of these factors pose
102 significant challenges to accurately simulating pollen emissions.

103 Therefore, this study constructs a pollen emissions model for the Beijing area,
104 leveraging pollen concentration and meteorological monitoring data, combined with
105 pollen phenology and the RF algorithm. It conducts a simulation study on the
106 emission phenology of three types of pollen in Beijing (Artemisia, Chenopod, and
107 total pollen concentrations) to calculate the pollen emissions potential. The study also
108 investigates the seasonal and spatiotemporal distribution characteristics of pollen in
109 Beijing and its potential correlations with meteorological factors and climatic
110 conditions. Additionally, the constructed pollen emissions parameterization method is
111 applied to the RegCM and evaluated for accuracy using 15 years of pollen
112 observation data. This comprehensive study will enhance the understanding of pollen
113 sources, provide innovative guidance for the selection and planting of greening plants,
114 and promote sustainable development in ecological protection and urban planning.

115 **2. Methodology**

116 *2.1 Model description*



117 2.1.1 Parameterization method for pollen emissions

118 This study's pollen emissions potential integrates geographical parameters,
119 vegetation types, and meteorological data, and incorporates autumn pollen phenology
120 and RF to enhance the simulation of pollen phenology. This approach is used to
121 predict pollen concentration and distribution within the seasonal cycle. The specific
122 calculation formula is as follows:

123

$$E_i(t) = f_i \cdot P_{annual,i} \cdot e^{-\frac{(t-\mu)^2}{2\delta^2}} \quad (1)$$

124 In the formula, $E_i(t)$ represents the pollen emissions potential for pollen type i on
125 day t of the year (DOY), t represents a specific day of the year, and i represents the
126 i -th type of pollen. f_i represents the vegetation land cover fraction, which is the
127 percentage of different vegetation types within a unit area, measured in %. $P_{annual,i}$
128 represents the production factor of the i -th vegetation type, which is the number of
129 pollen grains released during the pollen season, measured in $Grain\ m^{-2}\ year^{-1}$. In this
130 study, $P_{annual,i}$ is calculated based on the RF algorithm (Sect. 2.1.3). $e^{-\frac{(t-\mu)^2}{2\delta^2}}$
131 represents the phenological evolution of pollen emissions, controlling the pollen
132 release process. The formula indicates that pollen emissions during the pollen season
133 follows a Gaussian distribution, where μ and δ are the mean and standard
134 deviation of the Gaussian distribution. These parameters are calculated from sDOY
135 and eDOY of the pollen season, as follows:

136

$$\mu = \frac{sDOY + eDOY}{2} \quad (2)$$

137

$$\delta = \frac{eDOY - sDOY}{a} \quad (3)$$

138 In this context, sDOY and eDOY are optimized using autumn pollen phenology
139 (Sect. 2.1.2). The parameter a represents a fitting parameter that explains the
140 conversion between the empirical phenological dates based on pollen count thresholds
141 and the equivalent width of the emission curve. In this study, the value of a is set to 4.

142 This equation can be applied to a specific type of pollen or to the calculation of
143 pollen concentration over the entire pollen season, depending mainly on the land



144 cover type. The emission can be calculated offline using this equation or applied in
 145 online calculations.

146 2.1.2 Autumn pollen phenology model

147 In this study, we used three different calculation methods (RS_1 , RS_2 , RS_{sig}) for the
 148 autumn phenology model to simulate sDOY and eDOY of autumn pollen (Meier &
 149 Bigler, 2023). Each model is related to temperature and SSH. The specific calculation
 150 formulas are as follows:

$$151 \quad RS_1 = \begin{cases} (T_{base} - T_i)^x \times (L_i / L_{base})^y, & T_i < T_{base} \wedge L_i < L_{base} \\ 0 & , T_i \geq T_{base} \vee L_i \geq L_{base} \end{cases} \quad (4)$$

$$152 \quad RS_2 = \begin{cases} (T_{base} - T_i)^x \times (1 - L_i / L_{base})^y, & T_i < T_{base} \wedge L_i < L_{base} \\ 0 & , T_i \geq T_{base} \vee L_i \geq L_{base} \end{cases} \quad (5)$$

$$153 \quad RS_{sig} = \frac{1}{1 + e^{a(T_i \times L_i - b)}} \quad (6)$$

$$154 \quad \sum_{t_0}^{t_n} RS_i \geq Y \quad (7)$$

155 In the above equations, RS_1 , RS_2 and RS_{sig} represent three different autumn
 156 phenology model categories. T_i and L_i represent the temperature and SSH on a given
 157 day, respectively, while T_{base} and L_{base} represent the thresholds for temperature and
 158 SSH, respectively. In the RS_1 and RS_2 models, when the temperature and SSH are
 159 below the threshold or the date exceeds a fixed DOY, RS starts accumulating. In the
 160 RS_{sig} model, temperature and SSH accumulate inversely in an exponential form. The
 161 day t_n , when the cumulative amount exceeds the threshold Y , represents the final
 162 simulated pollen start/end date. t_0 represents the start day of accumulation, which is
 163 the first day when $T_i < T_{base}$ and $L_i < L_{base}$. The parameters that need to be adjusted are Y ,
 164 T_{base} , L_{base} , x , y and $start_day$. In this study, the simulated annealing algorithm is used
 165 for parameter adjustment. The principle of the simulated annealing (SA) algorithm is
 166 to simulate the random optimization process of the annealing process in solid-state
 167 physics, which can accept non-optimal solutions with a certain probability to avoid
 168 falling into local optima and eventually achieve the global optimum.

169 2.1.3 Random Forests



170 Random Forests (RF) is an ensemble learning algorithm introduced by Breiman
171 (2001) for classification and regression tasks. This algorithm enhances model
172 prediction performance and robustness by constructing multiple decision trees and
173 combining their outputs. The core principle involves drawing multiple sample sets
174 with replacement from the original training set, training a decision tree for each
175 sample set, and randomly selecting a subset of features at each node split to reduce
176 correlation between the trees. Ultimately, RF generates the final prediction by
177 averaging (for regression) or voting (for classification) the outputs of these trees. The
178 advantages of this method include high prediction accuracy, strong resistance to
179 overfitting, suitability for high-dimensional data, and efficient training processes. The
180 RF algorithm has been widely applied across various fields (Virro et al., 2022; Li et
181 al., 2023; Chen et al., 2024; Valipour Shokouhi et al., 2024).

182 In this study, the RF algorithm is employed to simulate annual pollen production.
183 Each pollen dataset is divided into training and testing sets in a 4:1 ratio, with the
184 training set used for model training and the testing set for accuracy validation.
185 Additionally, a grid search with cross-validation is applied to optimize the
186 hyperparameters of each estimator. Key parameters for RF adjustment include
187 `n_estimators`, `max_depth`, `min_samples_split`, and `min_samples_leaf`. Hyperparameter
188 optimization is a crucial step in enhancing model performance.

189 *2.2 Data*

190 *2.2.1 Observed pollen concentrations*

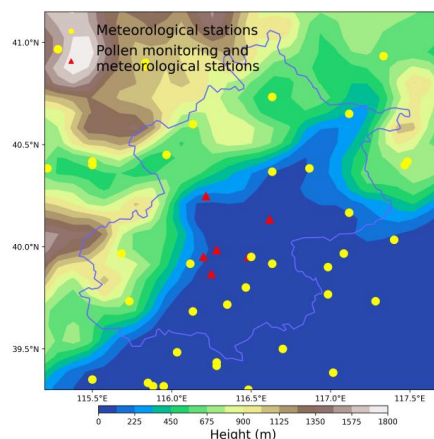
191 The daily pollen concentration data were collected from six monitoring stations
192 in Beijing: Changping (CP), Chaoyang (CY), Fengtai (FT), Haidian (HD),
193 Shijingshan (SJS), and Shunyi (SY), as shown in Fig. 1. The monitoring period
194 spanned from April to October each year from 2006 to 2021, covering the main pollen
195 season in Beijing. The gravitational settling method (Unit: 10^3 Grains $m^{-2} d^{-1}$) was
196 used for monitoring. The pollen concentration data included Total Pollen
197 Concentration (the sum of pollen concentrations from all taxa, abbreviated as TotalPC)
198 and the concentrations of pollen from 10 common allergenic plants. These species
199 included trees such as Pine, Poplar, Birch, Cypress, Ash, and Elm, as well as weeds



200 like Artemisia, Chenopod, Humulus, and Amaranthus. Although autumn pollen
201 concentrations are lower compared to spring, autumn weed pollen has a higher
202 allergenic potential (Zhao et al., 2023). Therefore, this study focuses on the analysis
203 of autumn weed pollen. Due to significant data gaps in the pollen concentration of
204 specific species, we selected only the data that were more complete and of higher
205 allergenic potential, specifically Artemisia, Chenopod, and TotalPC. Table 1 provides
206 basic information, such as the number of effective sample years for these three types
207 of pollen across the six stations.

208 To prevent anomalies in the data, we excluded outliers in the pollen
209 concentration data for each species and any data points where the concentration
210 exceeded the 99th percentile. Furthermore, we applied a 5-day moving average to the
211 pollen monitoring data to smooth it. This approach not only eliminates noise from the
212 data (Li et al., 2019; Li et al., 2022) but also mitigates the influence of daily
213 meteorological changes and advection diffusion on daily pollen emissions (To further
214 analyze the impact of key factors such as meteorological factors and advection
215 diffusion on daily pollen emissions, we used the RegCM in Sect. 3.3. This model
216 accurately reflects the effects of daily meteorological factors such as temperature,
217 precipitation, humidity, and wind speed on pollen emissions while also describing key
218 physical processes such as advection diffusion, convective transport, and dry and wet
219 deposition, thus providing a comprehensive analysis of the behavior of pollen in the
220 atmosphere). This smoothing process allows us to more clearly explore the daily
221 variation trends of pollen.

222 Additionally, to better simulate the temporal and spatial distribution of pollen
223 during the autumn pollen period, we defined the autumn pollen period based on
224 observed pollen concentration data as $DOY\ 215 < DOY < 280$. Subsequently, we
225 determined the Start Day of Year (sDOY) and End Day of Year (eDOY) for the
226 autumn pollen period for each station and year by identifying the day of year at which
227 the cumulative pollen concentration reached 5 % (start) and 95 % (end) of the total for
228 that period (Khwarahm et al., 2017; Li et al., 2019; Li et al., 2022).



229

230

Fig. 1. Distribution map of geopotential height, pollen observation stations (triangle), and

231

meteorological monitoring stations (circle) in Beijing area

232

Table 1 Explanation of effective sample years for pollen monitoring stations in Beijing

233

(2006-2021)

Station	Effective Sample Years / Year		
	Artemisia	Chenopod	TotalPC
CP	16	16	16
CY	13	13	13
FT	10	8	15
HD	0	0	8
SJS	11	11	16
SY	12	9	16
Total	62	57	84

234

To better simulate sDOY and eDOY for pollen, this study first applied the

235

Gaussian model to the autumn pollen data of each station and year. The Gaussian

236

model was chosen for its effectiveness in capturing peaks in time series data, which

237

are often reflected in pollen concentration data. Taking the CP station as an example,

238

Gaussian fitting distribution was performed on the autumn Artemisia, Chenopod, and

239

TotalPC for 2006-2021 (Supplementary Fig. S1-S3). The results indicated that the

240

autumn pollen concentration exhibited a significant Gaussian distribution, confirming

241

that the Gaussian model could aptly fit the time series changes of autumn pollen.



242 Therefore, by Gaussian fitting the pollen concentrations of each station, the autumn
243 pollen sDOY and eDOY under the Gaussian model simulation were further
244 determined. Comparing the sDOY and eDOY derived from observed pollen
245 concentration data with those obtained via Gaussian model simulation
246 (Supplementary Fig. S4), we found a high correlation coefficient (R) and a low root
247 mean square error (RMSE) between the two. Thus, the sDOY and eDOY obtained
248 from Gaussian model simulation were utilized to study the autumn pollen phenology.

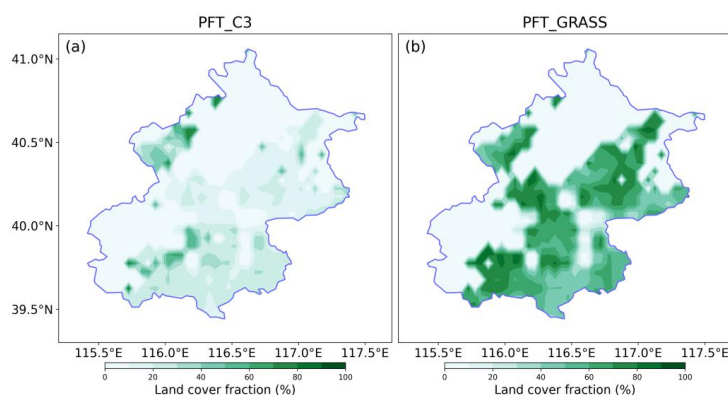
249 *2.2.2 Meteorological observation and land cover data*

250 The meteorological data for this study were sourced from the China Surface
251 Climate Daily Dataset, encompassing observations from all benchmark and basic
252 meteorological stations in China. Specifically, we utilized data from 66 valid
253 meteorological stations in Beijing and its surrounding areas (39-41.5° N, 115-118° E)
254 covering the period from 2006 to 2020 (Fig. 1). This dataset includes meteorological
255 observations corresponding to the pollen monitoring stations (our meteorological data
256 extends only up to 2020). The variables incorporated in this study comprise average
257 temperature (TEM_Avg), maximum temperature (TEM_Max), minimum temperature
258 (TEM_Min), sunshine hours (SSH), station altitude (Alti), average pressure
259 (PRS_Avg), maximum pressure (PRS_Max), minimum pressure (PRS_Min),
260 maximum wind speed (WIN_S_Max), extreme wind speed (WIN_S_Inst_Max),
261 average 2-minute wind speed (WIN_S_2mi_Avg), ground surface temperature
262 (GST_Avg_Xcm, X=5, 10, 15, 20, 40, 80, 160, 320cm), average ground surface
263 temperature (GST_Avg), minimum ground surface temperature (GST_Min),
264 maximum ground surface temperature (GST_Max), average relative humidity
265 (RHU_Avg), minimum relative humidity (RHU_Min), average vapor pressure
266 (VAP_Avg), precipitation from 20:00 to 20:00 (PRE_Time_2020), and precipitation
267 from 08:00 to 08:00 (PRE_Time_0808). The first four meteorological factors were
268 utilized to simulate the autumn phenology model of pollen, predicting various pollen
269 sDOY and eDOY. All meteorological factors served as training datasets for the RF
270 algorithm to simulate annual pollen production.

271 For land use data, this study employed the Community Land Model 4 (CLM4)



272 dataset (Oleson et al., 2010), which includes 25 plant functional types such as
273 needleleaf forests, broadleaf forests, shrubs, grasses (C3 and C4), and crops, with a
274 spatial resolution of 0.05°. As Artemisia and Chenopod primarily fall under the C3
275 plant category (Yorimitsu et al., 2019; Septembre-Malaterre et al., 2020; Qiao et al.,
276 2023), the simulation of pollen utilization for Artemisia and Chenopod used plant
277 functional C3 grass, while the TotalPC simulation incorporated both C3 and C4
278 grasses. The distribution of these two plant functional types in Beijing is illustrated in
279 Fig. 2.



280

281 Fig. 2. The distribution of plant functional type C3 (a) and GRASS (b) in Beijing area

282 3. Results and Discussion

283 3.1 Pollen Phenology Simulation

284 In this study, we analyzed the phenological changes of three types of
285 pollen—Artemisia, Chenopod, and TotalPC—during the autumn season based on
286 three different autumn pollen phenology calculation methods (Rs_1 , Rs_2 , and Rs_{sig}).
287 Specifically, we examined the seasonal phenological simulations of these pollen
288 concentrations under three different temperature conditions (TEM_Avg, TEM_Max,
289 and TEM_Min) (Mo et al., 2023), with a primary focus on sDOY and eDOY.
290 Additionally, the annual pollen production (P_{annual}) was simulated using the RF
291 algorithm.

292 3.1.1 Simulation of sDOY and eDOY based on autumn phenology model

293 Table 2 presents the statistical indicators for simulating the phenology of



294 Artemisia using different phenological methods and temperature conditions. For
295 simulating the sDOY for Artemisia, the Rs_1 , Rs_2 , and Rs_{sig} methods demonstrated high
296 accuracy when TEM_Avg and TEM_Min were employed as temperature conditions.
297 The R values for both the training and testing sets exceeded 0.45, with some R values
298 in the testing set surpassing 0.7, and the RMSE values were relatively low. This
299 indicates that these three methods effectively capture the phenological characteristics
300 of Artemisia at the onset of autumn. Notably, the Rs_{sig} method, when using TEM_Avg
301 as the condition, achieved R values of 0.53 and 0.80 for the training and testing sets,
302 respectively, with RMSE values of 6.61 and 4.86, showing the best simulation
303 performance. However, when TEM_Max was used as the temperature condition, the
304 simulation performance of all three methods declined. The R value of the Rs_1 method
305 fell below 0.2, and the RMSE values were high, exceeding 8 days. Comparatively, the
306 Rs_{sig} method performed slightly better but still yielded inferior results compared to
307 TEM_Avg and TEM_Min, indicating lower model stability when predicting Artemisia
308 sDOY with TEM_Max. For the simulation of Artemisia eDOY, the performance of the
309 three methods was relatively close, with R values in the training and testing sets
310 generally ranging from 0.3 to 0.5, and similar RMSE values. Among them, the Rs_1
311 method performed better when TEM_Min and TEM_Avg were used as temperature
312 conditions, with R values of 0.66 and 0.51 in the testing set and RMSE values of 3.32
313 days and 3.9 days, respectively. Compared to the Rs_1 method, the Rs_2 and Rs_{sig}
314 methods were relatively weaker in predicting eDOY, indicating that the Rs_1 method
315 better captures the phenological trends of Artemisia at the end of autumn. Additionally,
316 when comparing the simulation results of sDOY and eDOY, sDOY generally had
317 higher R values, but eDOY had lower overall RMSE values.

318 The statistical indicators for simulating the phenology of Chenopod under
319 different phenological methods and temperature conditions are shown in Table 3. For
320 the simulation of the sDOY for Chenopod, the Rs_1 and Rs_2 methods demonstrated
321 high accuracy when using TEM_Min and TEM_Avg as temperature conditions. The R
322 values for both the training and testing sets were around 0.5, and the RMSE values
323 were relatively low. It is clear that using TEM_Avg as the temperature condition



324 yields higher R values and lower RMSE (in the case of the Rs_1 method) compared to
325 TEM_Min, indicating that these two methods effectively capture the phenological
326 changes of Chenopod at the onset of autumn when using TEM_Avg as the
327 temperature condition. However, when TEM_Max was used as the temperature
328 condition, the simulation performance of all three methods declined, particularly for
329 Rs_1 , which had an R value of -0.1 and an RMSE greater than 9 days in the testing set.
330 The Rs_{sig} method, when using TEM_Avg, achieved an R value of 0.51 in the training
331 set but only 0.28 in the testing set, with a high RMSE of 5.32, indicating poor model
332 stability in this scenario. In contrast to TotalPC and Artemisia, the simulation of the
333 eDOY for Chenopod was not satisfactory for any of the three methods. The R values
334 for both the training and testing sets were all below 0.42. Particularly when using
335 TEM_Max as the temperature condition, the simulation performance of all three
336 methods was poor, with the testing set R value reaching only 0.1. This indicates that
337 the models have limited ability to capture the end of the autumn season for Chenopod.

338 Table 4 shows the phenological simulation statistical indicators of TotalPC under
339 different phenological methods and temperature conditions. From the data in the table,
340 it can be seen that for the simulation of the sDOY of TotalPC, all three phenological
341 methods (Rs_1 , Rs_2 , and Rs_{sig}) performed with high accuracy ($R > 0.5$) and relatively
342 low RMSE when using TEM_Min. This indicates that these three methods, when
343 using TEM_Min, can effectively capture the trend of the sDOY of TotalPC during the
344 autumn season. Meanwhile, the Rs_1 method also showed good simulation
345 performance when using TEM_Avg as the temperature condition, with R reaching
346 0.54 for both the training and testing sets. The Rs_{sig} method, using TEM_Avg, had
347 good simulation performance in the training set, but the R in the testing set only
348 reached 0.38. Compared to TEM_Min and TEM_Avg, the Rs_2 and Rs_{sig} methods
349 showed slightly inferior simulation performance when using TEM_Max as the
350 temperature condition. Surprisingly, the Rs_1 method's simulation of the sDOY showed
351 a negative correlation when using TEM_Max, indicating the worst performance. For
352 the simulation of the eDOY of TotalPC, the overall simulation performance was
353 worse in terms of R compared to sDOY, but the RMSE values were generally better.



354 Specifically, using TEM_Avg as the temperature condition, the RS_2 and RS_{sig} methods
 355 showed relatively good simulation performance and lower RMSE. However, the RS_2
 356 method performed much worse on the testing set compared to the training set, with
 357 the R on the testing set being only 0.32.

358 Overall, different pollen types exhibit varying sensitivity to different
 359 phenological models and temperature conditions. TEM_Avg is generally the best
 360 temperature condition for predicting the sDOY of the three pollen types, providing
 361 higher R values and lower RMSE. This suggests that TEM_Avg can effectively
 362 predict the start of the autumn pollen season. At the same time, TEM_Min also
 363 performs well in predicting the sDOY of TotalPC and Artemisia, whereas TEM_Max
 364 generally shows the poorest prediction performance. For predicting eDOY, different
 365 pollen types show different sensitivities to temperature conditions, but overall, the
 366 models perform worse for eDOY compared to sDOY, especially in the simulation of
 367 Chenopod.

368 Table2 Statistical indicators of Artemisia phenology under different phenological methods and
 369 temperature conditions

Artemisia		$RS_1(R)$		$RS_2(R)$		$RS_{sig}(R)$		$RS_1(RMSE)$		$RS_2(RMSE)$		$RS_{sig}(RMSE)$	
		Train	Test	Train	Test	Train	Test	Train	Test	Train	Test	Train	Test
sDOY	TEM_Min	0.47	0.66 [#]	0.52 [*]	0.77 [#]	0.45	0.59 [#]	6.61	5.93	6.29	4.99	6.63	6.57
	TEM_Avg	0.45	0.63 [#]	0.50	0.71 [#]	0.53[*]	0.80[#]	6.67	6.18	6.78	5.44	6.61	4.86
	TEM_Max	0.16	0.17	0.44	0.47	0.45	0.58 [#]	8.87	9.58	8.21	7.51	6.52	6.32
eDOY	TEM_Min	0.38	0.66[#]	0.38	0.44	0.36	0.37	4.19	3.32	4.19	3.97	4.02	4.07
	TEM_Avg	0.46	0.51 [*]	0.38	0.29	0.44	0.44	3.92	3.9	4.16	4.23	3.85	4.07
	TEM_Max	0.31	0.43	0.05	0.07	0.33	0.27	5.59	4.65	6.84	6.47	3.98	4.32

370 Table3 Statistical indicators of Chenopod phenology under different phenological methods and
 371 temperature conditions

Chenopod		$RS_1(R)$		$RS_2(R)$		$RS_{sig}(R)$		$RS_1(RMSE)$		$RS_2(RMSE)$		$RS_{sig}(RMSE)$	
		Train	Test	Train	Test	Train	Test	Train	Test	Train	Test	Train	Test
○	TEM_Min	0.42	0.44	0.59 [#]	0.36	0.47	0.36	4.68	5.09	4.12	5.28	4.38	5.25



	TEM_Avg	0.55*	0.47	0.63#	0.33	0.51	0.28	4.13	5.37	4.49	5.42	4.12	5.32
	TEM_Max	0.31	-0.1	0.43	0.28	0.42	0.18	7.84	9.13	5.66	5.9	5.55	6.06
	TEM_Min	0.42	0.25	0.17	0.2	0.26	0.11	4.23	4.94	4.31	4.71	4.15	4.75
eDOY	TEM_Avg	0.37	0.1	0.39	0.23	0.34	0.33	3.98	5.29	4.09	4.84	4.16	4.65
	TEM_Max	0.23	-0.0	0.27	-0.1	0.13	0.11	5.57	6.87	5.53	7.09	6.31	7.14

372 Table4 Statistical indicators of TotalPC phenology under different phenological methods and
 373 temperature conditions

TotalPC	Rs ₁ (R)		Rs ₂ (R)		Rs _{sig} (R)		Rs ₁ (RMSE)		Rs ₂ (RMSE)		Rs _{sig} (RMSE)		
	Train	Test	Train	Test	Train	Test	Train	Test	Train	Test	Train	Test	
sDOY	TEM_Min	0.52*	0.53#	0.59#	0.56#	0.58#	0.55#	5.84	5.32	5.51	5.32	5.61	5.6
	TEM_Avg	0.54#	0.54#	0.08	nan	0.59#	0.45	5.89	5.21	6.75	6.27	5.71	5.62
	TEM_Max	-0.21	-0.19	0.51*	0.48*	0.52*	0.4	9.04	9.2	7.66	6.45	5.83	6.1
eDOY	TEM_Min	0.41	0.21	0.35	0.24	0.5*	0.36	4.76	4.47	4.9	4	4.75	3.41
	TEM_Avg	0.51*	0.18	0.63#	0.32	0.5*	0.49*	4.47	4.83	4.4	3.95	4.63	3.11
	TEM_Max	0.44	0.4	0.18	0.2	0.39	0.29	6.41	6.47	7.7	6.56	4.78	3.72

374 Note: Bold represents the best model performance, # Indicates significance levels at P < 0.001, *

375 Indicates significance levels at P < 0.005

376 Based on the above discussion, we selected the most suitable phenological and
 377 temperature conditions for the three types of pollen (bold parts in Table 2-4),
 378 simulated their sDOY and eDOY, and generated line and scatter plots (Fig. 3).
 379 According to the line plots in Fig. 3 (top), the predicted results for Artemisia are the
 380 closest to the actual observed results. The predictions for TotalPC follow, while the
 381 predictions for Chenopod show some deviation, particularly in eDOY, indicating the
 382 need for a more suitable phenological model to accurately simulate the phenology of
 383 Chenopod. The scatter plots in Fig. 3 (bottom) illustrate that for sDOY predictions,
 384 Artemisia exhibited the strongest correlation between predicted and observed pollen
 385 phenology, with an R value of 0.69 and an RMSE of 5.77 days. In contrast, Chenopod
 386 had the lowest correlation, with an R value of 0.49 and an RMSE of 4.98 days. It can
 387 also be observed that higher R values are associated with higher overall RMSE,



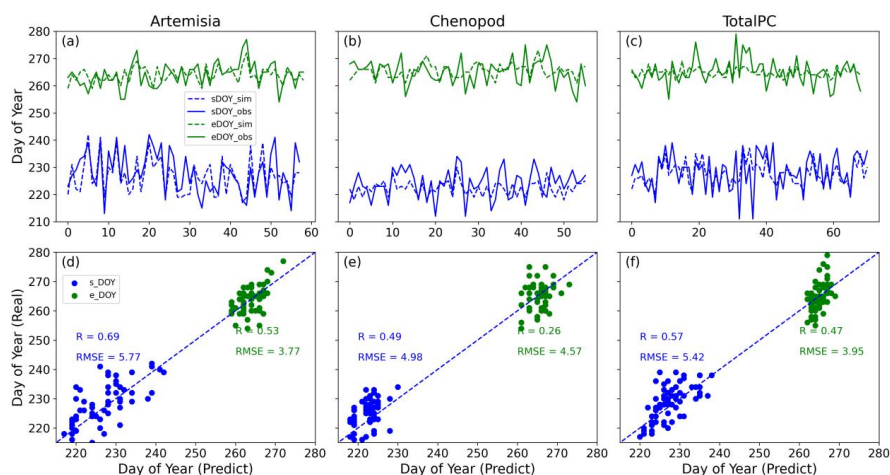
388 possibly due to the models being more sensitive to noise or outliers in the data, which
389 increases the overall error. For high-correlation predictions like those for Artemisia,
390 the model may be more affected by random fluctuations in the data, leading to
391 increased error. Additionally, different pollen types may exhibit varying
392 characteristics or response patterns in phenological models, resulting in a non-linear
393 or inconsistent relationship between correlation and error. For eDOY predictions, the
394 correlation between predicted and observed is highest for Artemisia, with an R value
395 of 0.53 and an RMSE of 3.77 days. Chenopod has the lowest correlation for eDOY
396 predictions, with an R value of only 0.26 and an RMSE of 4.57 days. The poorer
397 performance in simulating eDOY for Chenopod may be due to lower data quality
398 compared to Artemisia and TotalPC, as well as the smallest sample size, resulting in
399 insufficient information and samples for the model to learn and predict accurately.

400 Additionally, Table 5 shows the proportion of simulations with errors less than 5
401 days and 3 days for sDOY and eDOY across the three pollen types. It can be seen that
402 the proportion of eDOY simulations with errors less than 5 days and 3 days is higher
403 than that for sDOY, indicating that eDOY simulations generally have better accuracy
404 in terms of error. Specifically, for Chenopod eDOY simulations, although the R value
405 is poor, 76.79 % of simulations have errors less than 5 days, and 55.36 % have errors
406 less than 3 days, meaning that more than half of the eDOY simulations have errors
407 within 3 days. This performance is comparable to the other two pollen types (64.41 %
408 and 68.12 %, respectively). Compared to Mo et al. (2023), which simulated the spring
409 season start pollen season (SPS) using 17 phenological models, this study has slightly
410 lower R values but much lower RMSE (around 11 days in their study). Li et al. (2022)
411 used satellite data to simulate the SPS for Birch, Oak, and Poplar, achieving RMSE
412 values between 4.26 and 8.77 days. Furthermore, this study's process-based
413 phenological models for sDOY and eDOY show smaller errors and higher
414 correlations compared to empirical linear models based solely on temperature used by
415 Wozniak and Steiner (2017) and Zhang and Steiner (2022).

416 Therefore, from an error analysis perspective, the simulation performance of
417 Chenopod eDOY maintains a relatively low error while also demonstrating some



418 stability, indicating that the autumn phenological model can accurately capture the
 419 seasonal variation trend of Chenopod. This makes the simulation results reliable.
 420 Overall, the autumn phenological models provide good simulation performance for
 421 the phenology of the three pollen types, laying a solid foundation for further analysis
 422 of pollen temporal characteristics.



423
 424 Fig. 3. Comparison of pollen sDOY and eDOY in autumn phenology: simulation vs. observation.
 425 Line plots of three different pollen sDOY and eDOY (a-c) and scatter plot comparison of the same
 426 (d-f). Specific comparisons for Artemisia (a, d), Chenopod (b, e), and TotalPC (c, f).

427 Table 5 Statistics on the proportion of errors between simulation and observation of three different
 428 types of pollen sDOY and eDOY within 5 and 3 days

	DOY	Artemisia (%)	Chenopod (%)	TotalPC (%)
<5D	sDOY	68.97	73.21	71.83
	eDOY	86.44	76.79	82.61
<3D	sDOY	48.28	44.64	53.52
	eDOY	64.41	55.36	68.12

429 Based on the temperature and SSH observational station data from the Beijing
 430 area, we interpolated the station data into a grid dataset with a horizontal resolution of
 431 0.1°. Using the selected autumn phenological models, we then performed gridded

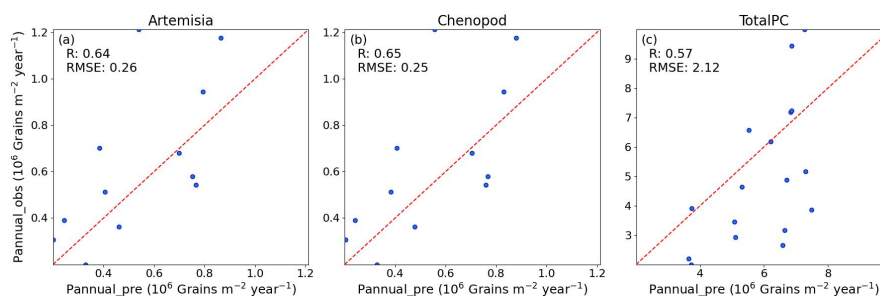


432 simulations of the sDOY and eDOY for three pollen types. This approach enabled us
433 to map the regional distribution of autumn pollen sDOY and eDOY in Beijing from
434 2006 to 2020, thereby laying the groundwork for further simulations of autumn pollen
435 emissions potential.

436 3.1.2 Simulation of annual pollen production based on RF

437 The simulation of annual pollen production (P_{annual} , referring to the cumulative
438 pollen concentration during each autumn pollen season) was conducted using the RF
439 algorithm. The training data comprised all station-observed pollen data from Table 1
440 and the corresponding meteorological observation data from Sect. 2.2.2. Four-fifths of
441 the station data were randomly selected as the training set to train the RF algorithm,
442 while the remaining one-fifth was used as the test set to validate the accuracy of the
443 RF's P_{annual} simulation. Fig. 4 presents the scatter plots of observed versus simulated
444 P_{annual} for three different pollen types (Artemisia, Chenopod, and TotalPC) based on
445 the RF in the test set. The R between simulated and observed values for the three
446 pollen types were all above 0.5, with Chenopod reaching 0.65. The calculated RMSE
447 was around 0.2×10^6 Grains m^{-2} year $^{-1}$ (with TotalPC having an RMSE of 2.12×10^6
448 Grains m^{-2} year $^{-1}$). This indicates that the prediction performance of the RF varies
449 among different pollen types, with the best performance for Chenopod and the poorest
450 for TotalPC annual production. Compared to the temperature-based empirical linear
451 models for P_{annual} by Zhang and Steiner (2022), the machine learning algorithm-based
452 simulations in this study have smaller errors and higher correlations. Overall, the RF
453 effectively simulates P_{annual} .

454 Based on meteorological observation data from stations in and around Beijing,
455 the station data were interpolated into a gridded dataset with a horizontal resolution of
456 0.1° . Subsequently, all station data for each pollen type were used as the training set,
457 with 12 stations in the gridded dataset cyclically selected as the test set for gridded
458 simulations. This ultimately resulted in the spatial distribution of P_{annual} in Beijing
459 from 2006 to 2020, laying the foundation for further simulation of autumn pollen
460 emissions potential.



461

462 Fig. 4. Scatter plots of simulated and observed annual pollen (P_{annual}) based on RF. Comparisons
463 for Artemisia (a), Chenopod (b), and TotalPC (c).

464 3.2 Simulation of Pollen Emissions in Beijing Area

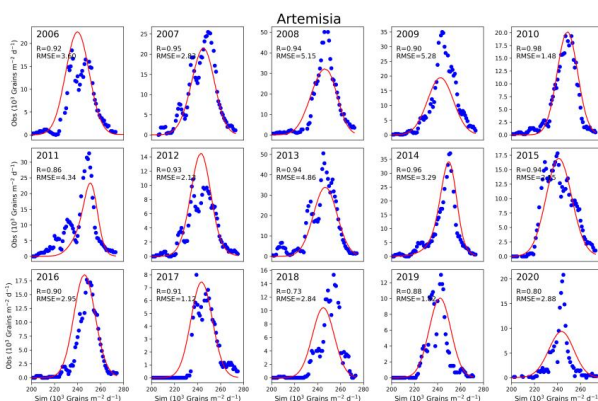
465 Based on the simulation results of autumn pollen phenology (sDOY, eDOY, and
466 P_{annual}) from Sect. 3.1 and the pollen emissions potential parameterization method
467 from Sect. 2.1.1, this study calculated the pollen emissions potential in the Beijing
468 area. Fig. 5-7 present a comparison between the observed and simulated average site
469 values of Artemisia, Chenopod, and TotalPC in Beijing from 2006 to 2020. In these
470 figures, blue dots represent the actual daily observed pollen counts, and red lines
471 represent the simulated pollen emissions. To assess the consistency between the
472 simulated and observed data, we calculated R and RMSE. As illustrated in the figures,
473 the simulated data closely match the actual observations in most years, with
474 correlation coefficients around 0.9. Specifically, the Artemisia emissions in 2010,
475 Chenopod emissions in 2016, and TotalPC emissions in 2007, 2009, 2018, and 2019
476 show R values as high as 0.98 and relatively low RMSE levels, demonstrating the
477 high accuracy of this study in simulating pollen emissions potential.

478 Additionally, the simulation results for sDOY and eDOY were also satisfactory,
479 though there were slight advances in the start of the pollen season in certain years,
480 such as 2017 and 2018 for Artemisia and Chenopod. While the peak pollen emissions
481 simulations were highly accurate in most years, there were instances of
482 overestimation and underestimation in some years. For example, the peak emissions
483 of Artemisia in 2008, 2009, and 2020, Chenopod in 2007, and TotalPC in 2013 and
484 2020 were significantly underestimated. Conversely, the peak simulations of TotalPC
485 in 2011 and 2012 were slightly overestimated. This indicates that, despite the high

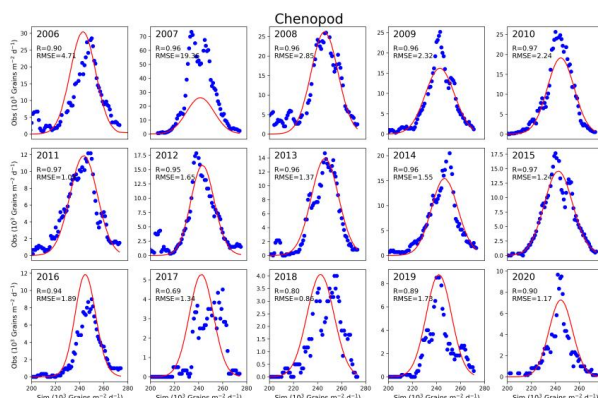


486 accuracy of the annual pollen production simulations based on the RF, there is still
487 room for improvement

488 Overall, this study achieved significant results in simulating pollen emissions,
489 demonstrating the potential application of autumn phenological models and the RF
490 algorithm in simulating pollen emissions. However, to further enhance the accuracy of
491 these simulations, future research needs to investigate and address the instances of
492 overestimation and underestimation in greater detail.



493
494 Fig. 5. Time series of observation and simulation of average Artemisia emissions at stations in
495 Beijing from 2006 to 2020. The red solid line represents the simulation of pollen emissions model,
496 while blue dots depict observations

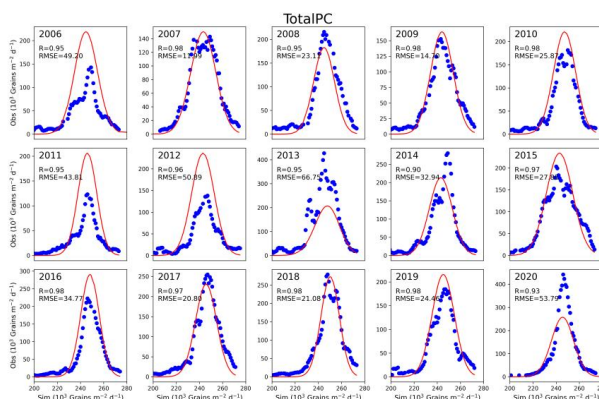


497
498 Fig. 6. Time series of observation and simulation of average Chenopod emissions at stations in
499 Beijing from 2006 to 2020. The red solid line represents the simulation of pollen emissions model,



500

while blue dots depict observations



501

502 Fig. 7. Time series of observation and simulation of average TotalPC emissions at stations in
503 Beijing from 2006 to 2020. The red solid line represents the simulation of pollen emissions model,

504

while blue dots depict observations

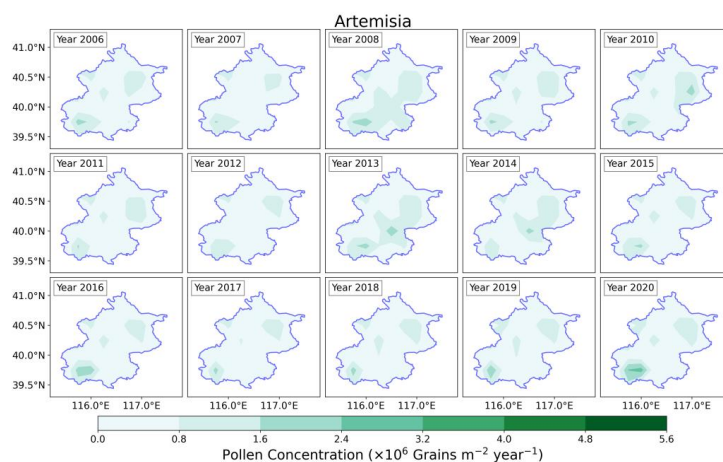
505

506 To further investigate the spatial distribution of annual pollen production, we
507 simulated the spatial distribution of annual Artemisia, Chenopod, and TotalPC
508 production in Beijing from 2006 to 2020 (Fig. 8-10). The results reveal significant
509 spatial and temporal variations in annual pollen production. Spatially, Artemisia
510 production is predominantly concentrated in the southeastern, northeastern, and
511 certain northwestern regions of Beijing, with occasional occurrences in the central
512 urban area during specific years (2008 and 2013). Chenopod production is highest in
513 the southern part of Beijing and lowest in the northern parts and surrounding areas.
514 Notably, from 2006 to 2008, the southern region exhibited high concentrations of
515 Chenopod production. TotalPC is mainly distributed in the southeastern plains of
516 Beijing, forming a strip-like pattern, while lower production is observed in the
517 northwestern mountainous areas, indicating a possible influence of geographical
518 location on TotalPC distribution. Temporally, the annual production of these three
519 pollen types demonstrates distinct interannual variations. Artemisia shows little
520 change in both distribution area and production concentration over time. In contrast,
521 Chenopod and TotalPC exhibit a general declining trend, reaching their lowest levels
522 between 2016 and 2018, which may be attributed to recent climatic changes,



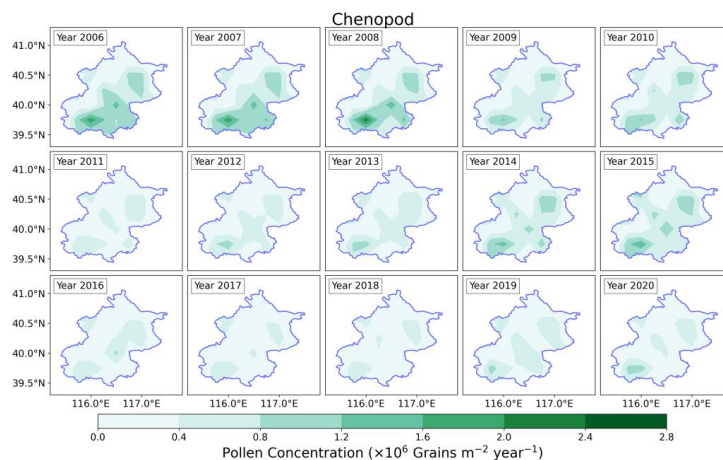
522 vegetation shifts, and human activities in the Beijing area.

523 The simulation results for annual pollen production of Artemisia, Chenopod, and
524 TotalPC in Beijing from 2006 to 2020, based on autumn phenology and the RF pollen
525 emissions model, indicate pronounced spatial differences and temporal variation
526 characteristics. Analyzing the spatial distribution and temporal variation of annual
527 pollen production in Beijing enhances our understanding of the spatiotemporal
528 patterns of pollen in the region, providing crucial insights for the control and
529 mitigation of pollen allergies.



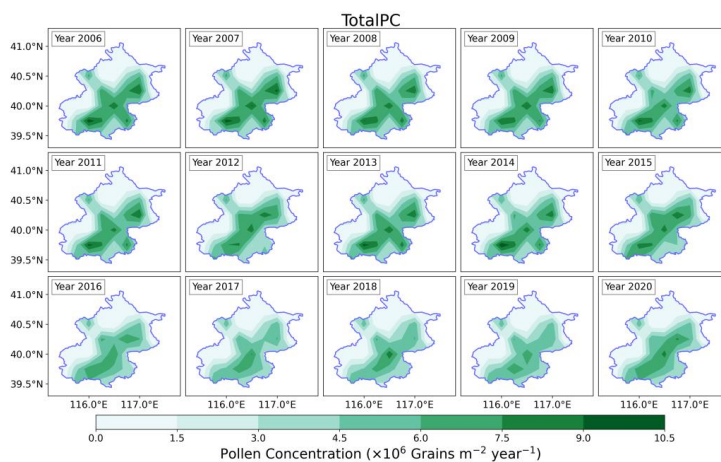
530

531 Fig. 8. Distribution of Artemisia in Beijing from 2006 to 2020 based on pollen emissions model



532

533 Fig. 9. Distribution of Chenopod in Beijing from 2006 to 2020 based on pollen emissions model



534

535 Fig. 10. Distribution of TotalPC in Beijing from 2006 to 2020 based on pollen emissions model

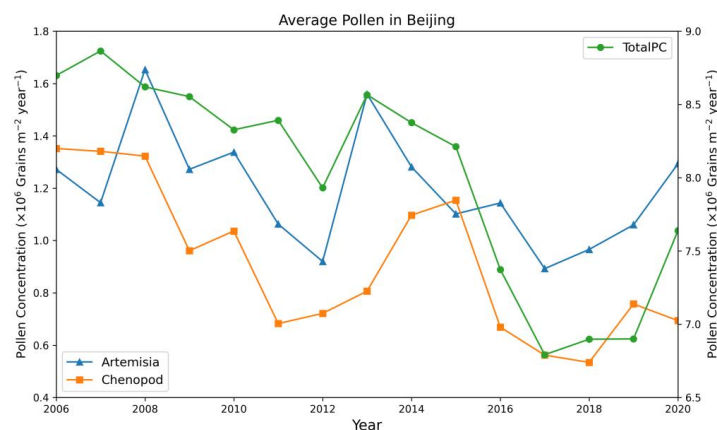
536 To more intuitively reflect the temporal variation trends in the annual production
537 of three types of pollen, we further analyzed the interannual variation of the regional
538 average cumulative concentration of these pollen types during the autumn pollen
539 season in Beijing from 2006 to 2020 (Fig. 11). The annual production of Artemisia,
540 Chenopod, and TotalPC in Beijing averages between 0.8-1.6, 0.5-1.4, and 6.5-9 grains
541 m⁻² year⁻¹, respectively. The annual production of Artemisia and Chenopod are
542 notably similar. Over time, the regional annual production of these pollen types in
543 Beijing exhibits significant fluctuations. Nonetheless, Artemisia remains relatively
544 stable, whereas Chenopod and TotalPC production demonstrate a discernible
545 declining trend, particularly in TotalPC. The annual production of all three pollen
546 types reached a local nadir in 2012. Following a surge in 2013, production steadily
547 declined from 2014 to 2017, reaching the lowest levels observed in nearly 15 years
548 (with TotalPC being the lowest in 2018). Subsequently, from 2018 to 2020, an
549 increasing trend was observed. Overall, the annual pollen production in Beijing
550 appears to follow a minor cyclical pattern, intimately linked to the impacts of climate
551 change.

552 To further explore the meteorological factors influencing average annual pollen
553 production in Beijing, we selected six meteorological variables during the autumn
554 pollen season from 2006 to 2020 for temporal and regional average calculations.



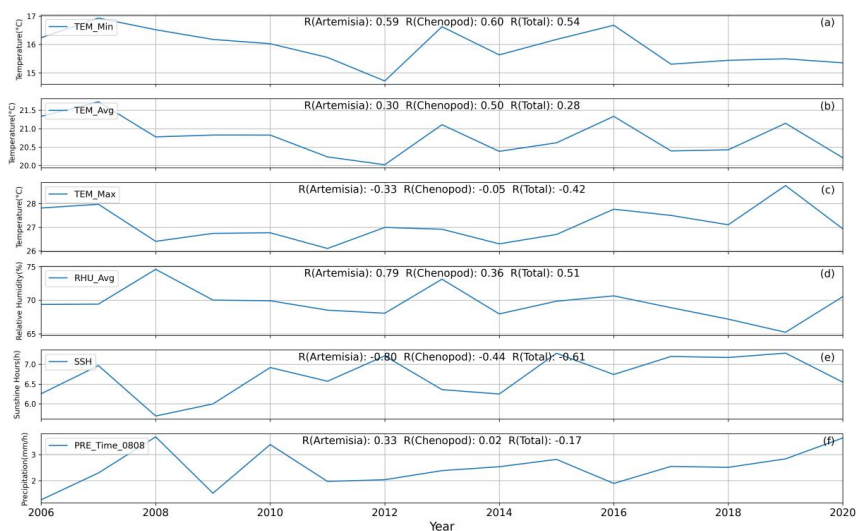
555 These factors include maximum temperature (TEM_Max), average temperature
556 (TEM_Avg), minimum temperature (TEM_Min), average relative humidity
557 (RHU_Avg), sunshine hours (SSH), and precipitation time (PRE_Time_0808). The
558 annual variations of these meteorological factors were analyzed, and their correlations
559 with annual pollen production variations were calculated (Fig. 12).

560 The trends in annual variations of each meteorological factor and the calculated
561 correlations reveal that for Artemisia, TEM_Min and RHU_Avg have a significant
562 positive correlation with its production, especially RHU_Avg, which shows a
563 correlation of 0.79. This indicates that an increase in relative humidity promotes
564 Artemisia production. Conversely, SSH has a correlation of -0.8 with Artemisia,
565 indicating that longer sunshine hours inhibit its production. Meanwhile, TEM_Avg
566 and PRE_Time_0808 have minor promoting effects on Artemisia production, while
567 TEM_Max has a slight inhibitory effect. For Chenopod, TEM_Min is the most
568 significant promoting factor, while SSH has an inhibitory effect, although its negative
569 correlation is lower than that for Artemisia, indicating a limited inhibitory effect on
570 Chenopod production. For TotalPC, similar to Artemisia, increases in TEM_Min and
571 RHU_Avg promote production, while increases in SSH and TEM_Max inhibit
572 production. Notably, the three types of pollen reached local minimum concentrations
573 in 2012, 2017, and 2018, when TEM_Min and SSH respectively reached local
574 minimum and maximum values, further demonstrating the promoting effect of
575 TEM_Min and the inhibitory effect of SSH on annual average pollen concentration.
576 Rahman et al. (2020) and Lei et al. (2023) indicated that temperature is the main
577 factor affecting the interannual variation of pollen and is positively correlated with
578 pollen production. Our findings are largely consistent with these conclusions,
579 although they did not consider the effect of SSH on interannual changes in pollen
580 concentration. In summary, the annual production of pollen in Beijing is significantly
581 influenced by meteorological conditions, particularly temperature, relative humidity,
582 and sunshine hours. Different meteorological factors exhibit distinct promoting and
583 inhibiting effects on pollen production.



584

585 Fig. 11. Time series variation chart of regional average annual production of three types of pollen
 586 in Beijing from 2006 to 2020



587

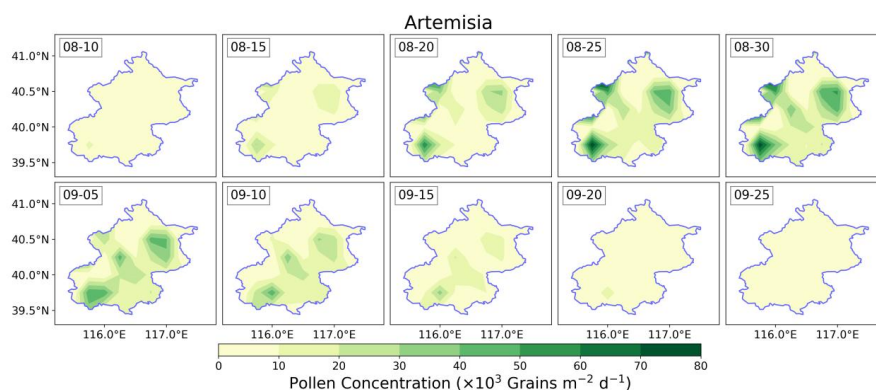
588 Fig. 12. Time series variation chart of average values of different meteorological factors in Beijing
 589 from 2006 to 2020. (The correlation coefficient between the average meteorological factors and
 590 the regional average annual production of three types of pollen is calculated in the figure)

591 Fig. 13-15 illustrate the spatial distribution of the average concentrations of
 592 Artemisia, Chenopod, and TotalPC during the autumn pollen season in Beijing from
 593 2006 to 2020. During this period, the concentration of all three pollen types initially
 594 increases and then decreases. The pollen season begins around August 10 each year
 595 and concludes around September 25. The peak concentrations for Artemisia and



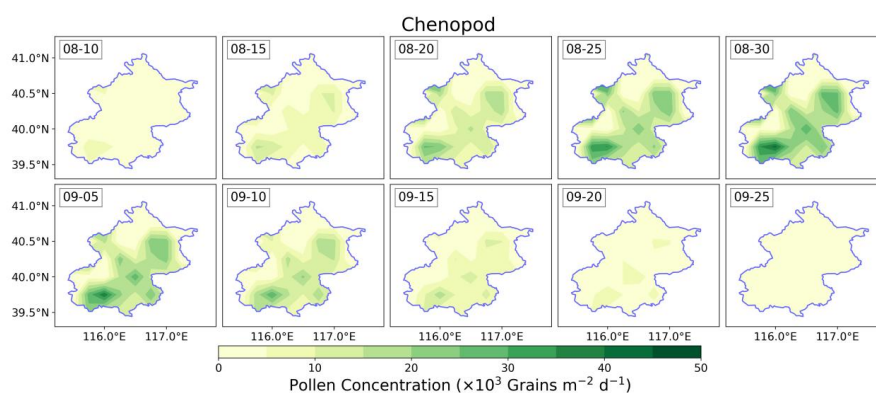
596 Chenopod pollen occur around August 30, while the peak concentration for TotalPC is
597 observed around September 5. The entire pollen season lasts approximately 45 days.

598 Regarding the average pollen concentration distribution, Artemisia is primarily
599 concentrated in the southwest, northeast, and parts of the northwest of Beijing, with
600 lower concentrations in the southeast. In contrast, Chenopod and TotalPC are mainly
601 distributed in the southeastern plains. The maximum average concentrations for
602 Artemisia, Chenopod, and TotalPC reach 81.1×10^3 Grains $m^{-2} d^{-1}$, 42.0×10^3 Grains
603 $m^{-2} d^{-1}$, and 351.8×10^3 Grains $m^{-2} d^{-1}$, respectively.



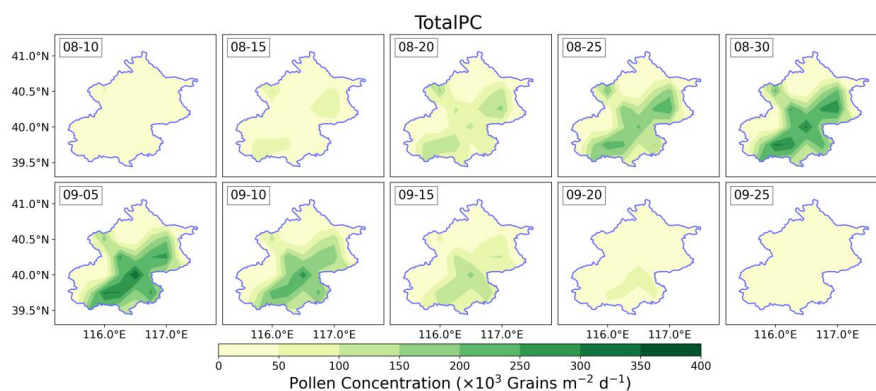
604

605 Fig. 13. Temporal and spatial distribution of Artemisia in Beijing (average from 2006 to 2020)



606

607 Fig. 14. Temporal and spatial distribution of Chenopod in Beijing (average from 2006 to 2020)



608

609 Fig. 15. Temporal and spatial distribution of TotalPC in Beijing (average from 2006 to 2020)

610 3.3 Simulation of Pollen Emissions in Regional Climate Models

611 To evaluate the pollen emissions model based on autumn pollen phenology and
612 RF, this study integrates the offline calculated pollen emissions into the regional
613 climate model RegCM. By comparing the simulated atmospheric pollen
614 concentrations with data from ground-based pollen monitoring stations, we assess the
615 performance of this pollen emissions potential model.

616 3.3.1 Implementation of pollen emissions in Regional Climate Model (RegCM)

617 RegCM is the pioneering regional climate model system used for climate
618 downscaling, originating in the late 1980s and early 1990s at the National Center for
619 Atmospheric Research (NCAR) in the USA. It has since undergone several
620 development iterations and is currently maintained at the International Centre for
621 Theoretical Physics (ICTP) in Italy. This open-source system is widely utilized by
622 numerous research teams, forming an extensive network for regional climate research.
623 The model can be applied globally and is evolving into a fully coupled regional earth
624 system model, incorporating ocean, lake, aerosol, desert dust, chemistry, hydrology,
625 and land surface processes. The version used in this study is RegCM4.7.1.

626 In this model, a pollen emissions model based on phenology and RF calculates
627 the emission potential of different types of pollen offline, and then incorporated into
628 the RegCM model. The calculation of pollen concentration in this model follows the
629 method of Sofiev et al. (2013), with the formula as follows:



630
$$E_{pollen,i}(t) = E_i(t) \cdot u_{star} \cdot ce \cdot f_w \cdot f_r \cdot f_h / htc \quad (8)$$

631
$$f_w = 1.5 - \exp(-(u_{10} + u_{conv}) / 5)$$

$$f_r = \begin{cases} 1, pr < pr_{low} \\ \frac{pr_{high} - pr}{pr_{high} - pr_{low}}, pr_{low} < pr < pr_{high} \\ 0, pr > pr_{high} \end{cases} \quad (9)$$

$$f_h = \begin{cases} 1, rh < rh_{low} \\ \frac{rh_{high} - rh}{rh_{high} - rh_{low}}, rh_{low} < rh < rh_{high} \\ 0, rh > rh_{high} \end{cases}$$

632 Where f_w , f_r and f_h represent the wind, precipitation, and RH factors,
 633 respectively, influencing pollen emissions concentration. u_{star} is surface friction
 634 velocity, ce is flowering factor, and htc is canopy height. f_w is exponentially related to
 635 the 10m wind speed u_{10} and vertical turbulent wind speed u_{conv} . pr and rh represent
 636 precipitation and RH. When precipitation is below the threshold pr_{low} , the
 637 precipitation factor is 1. When precipitation exceeds the threshold pr_{high} , the factor is 0.
 638 When precipitation is between these thresholds, the factor is calculated as the ratio of
 639 the difference between the high threshold and precipitation to the difference between
 640 the thresholds, with default values $pr_{low}=10^{-5}$ mm and $pr_{high}=0.5$ mm. Similarly, the
 641 RH factor is related to RH and its thresholds, with default values $rh_{low}=50$ % and
 642 $rh_{high}=80$ %. These factors explain the impact of wind, precipitation, and humidity on
 643 pollen emissions. Given the significant influence of precipitation and RH on pollen
 644 emissions, this study adjusts pr_{high} and rh_{high} values to 1 mm and 90 %, respectively.
 645 Higher thresholds can prevent excessive suppression of pollen emissions under
 646 frequent precipitation and high humidity conditions, thus more accurately simulating
 647 actual pollen concentration changes and better adapting the model to different climatic
 648 conditions.

649 Moreover, the RegCM includes the pollen tracer transport equation (Solmon et al.
 650 2006), as follows:

651
$$\frac{\partial \chi}{\partial t} = \bar{V} \cdot \nabla \chi + F_H + F_V + T_C + S - R_{wis} - R_{wc} - D_d \quad (10)$$

652 Where χ represents the tracer, F_H and F_V represent horizontal and vertical



653 diffusion, T_C represents convective transport, $RWls$ and RWc represent large-scale and
654 convective precipitation wet removal processes, respectively, and Dd represents dry
655 removal processes. This transport equation comprehensively considers various
656 physical processes and removal mechanisms of pollen in the atmosphere, allowing the
657 simulation of the entire process from pollen release to atmospheric dispersion and
658 deposition. This provides a foundation for fully describing the spatial distribution and
659 temporal evolution of pollen in the atmosphere, which is crucial for studying pollen
660 dispersion in the air, determining the spatial distribution of pollen concentration, and
661 predicting future changes in pollen concentration.

662 3.3.2 Evaluation of pollen simulation accuracy in RegCM

663 Fig. 16-18 depict the time series distribution of the concentrations of three pollen
664 types simulated by the RegCM compared to observed concentrations from 2006 to
665 2020. The RegCM successfully captures the temporal variation trends of pollen
666 concentrations during the autumn pollen season, generally showing an initial increase
667 followed by a decrease. Daily pollen concentrations fluctuate significantly due to
668 meteorological factors such as temperature, precipitation, and RH, as well as key
669 physical processes like advection, convection, and dry and wet deposition. Overall,
670 the simulated pollen concentrations by the RegCM align well with the observed trends,
671 though some discrepancies remain.

672 In the simulation of Artemisia (Fig. 16), the sDOY and pollen production vary
673 annually due to meteorological conditions and key physical processes. The annual
674 peak pollen concentrations generally range from $20\text{-}70 \times 10^3$ Grains $\text{m}^{-2} \text{d}^{-1}$, while in
675 2019-2020, observed pollen concentrations exceeded 100×10^3 Grains $\text{m}^{-2} \text{d}^{-1}$, with
676 notable spikes and drops likely due to abrupt meteorological changes or possible
677 issues with the quality of observation data. The RegCM accurately simulates the
678 sDOY and eDOY, displaying a similar frequency to observations. For peak pollen
679 simulations, years such as 2006, 2007, 2010, 2012, 2015, and 2016 show good
680 performance, with R above 0.7, particularly in 2006 and 2016, where R exceeds 0.85
681 and RMSE is only 4×10^3 Grains $\text{m}^{-2} \text{d}^{-1}$. However, for other years, peak simulations
682 are underestimated to varying degrees. For 2011, although the trend is consistent, the



683 observed peak is near 50×10^3 Grains $\text{m}^{-2} \text{d}^{-1}$, while the simulated peak is only 12×10^3
684 Grains $\text{m}^{-2} \text{d}^{-1}$, indicating a significant underestimation. This underestimation is also
685 noticeable in 2008, 2013, and 2017-2020. In 2019, although the peak concentrations
686 align, the trend correlation is low ($R=0.49$), and RMSE is high. The variability in
687 observation station data quality and quantity could influence these results, with some
688 years having fewer than six effective stations (minimum of two), impacting the
689 average and peak values. Box plots (Fig. 19) reveal that Artemisia concentrations in
690 2019-2020 are more dispersed, suggesting possible anomalies in observation data.
691 Overall, the R for RegCM simulations ranges from 0.69 to 0.86 (except 2019), with
692 RMSE between 3.05 - 15.38×10^3 Grains $\text{m}^{-2} \text{d}^{-1}$.

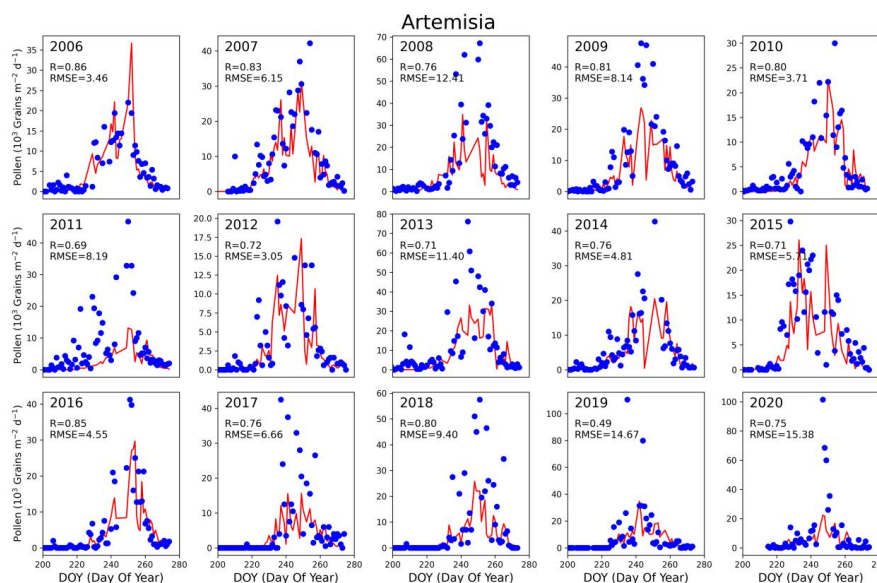
693 For Chenopod simulations (Fig. 17), the overall performance is similar to
694 Artemisia. The annual peak concentrations are generally lower, around 20 - 50×10^3
695 Grains $\text{m}^{-2} \text{d}^{-1}$, except for 2007, which reaches 120×10^3 Grains $\text{m}^{-2} \text{d}^{-1}$. The years
696 2006, 2008-2009, 2012-2013, 2015, and 2019 show good simulation performance,
697 accurately reflecting peak concentrations, particularly in 2016 ($R=0.84$,
698 $\text{RMSE}=3.11 \times 10^3$ Grains $\text{m}^{-2} \text{d}^{-1}$). However, 2007, 2010, 2017-2018, and 2020 exhibit
699 underestimation, with the exceptionally high observed concentrations in 2007 likely
700 causing the model's underestimation. Fig. 19 indicates increasing peak concentrations
701 in recent years (2017-2020) for both Artemisia and Chenopod, with room for
702 improvement in peak simulations by the RegCM. Despite the lower concentrations
703 compared to spring pollen, autumn pollen significantly impacts pollen-induced
704 diseases (pollinosis), prompting more attention and efforts in pollen management,
705 which contributes to the decreasing trend in monitored pollen concentrations.

706 TotalPC generally exhibits higher concentration levels compared to Artemisia
707 and Chenopod (Fig. 18). Annual peak TotalPC can reach 150 - 500×10^3 Grains $\text{m}^{-2} \text{d}^{-1}$,
708 with the highest observed concentration in 2020 at 745×10^3 Grains $\text{m}^{-2} \text{d}^{-1}$. Due to the
709 higher quality and completeness of TotalPC monitoring data, the simulation results
710 are more accurate, with R generally above 0.76 (except 2015, $R=0.64$). Over 60 % of
711 the years have R above 0.8, with fewer years showing significant underestimation of
712 peak concentrations (e.g., 2013). This highlights the critical role of high-quality

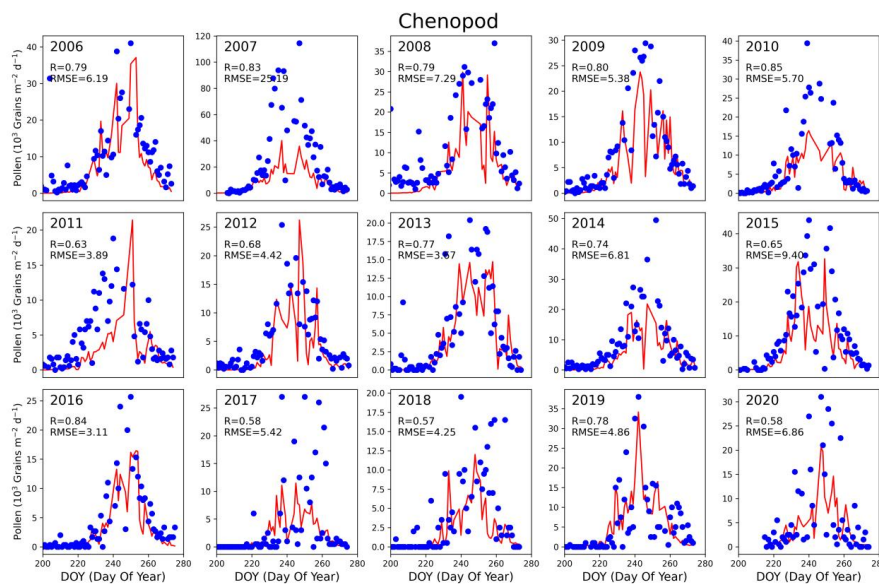


713 pollen monitoring data for accurate simulations. High-quality data enable precise
714 capturing of pollen concentration trends and peaks, providing robust support for
715 regional pollen phenology research.

716 In summary, the RegCM demonstrates high accuracy in simulating the
717 concentrations of the three pollen types, especially TotalPC. Accurate simulations of
718 pollen concentrations and peaks enhance the effectiveness of pollen emissions models,
719 improve health risk warnings, and provide a scientific basis for urban planning and
720 environmental management.



721
722 Fig. 16. Time-series distribution of Artemisia under RegCM simulation compared to observations
723 (averaged across effective pollen monitoring sites). The red solid line represents model
724 simulations, while blue dots depict observations



725

726

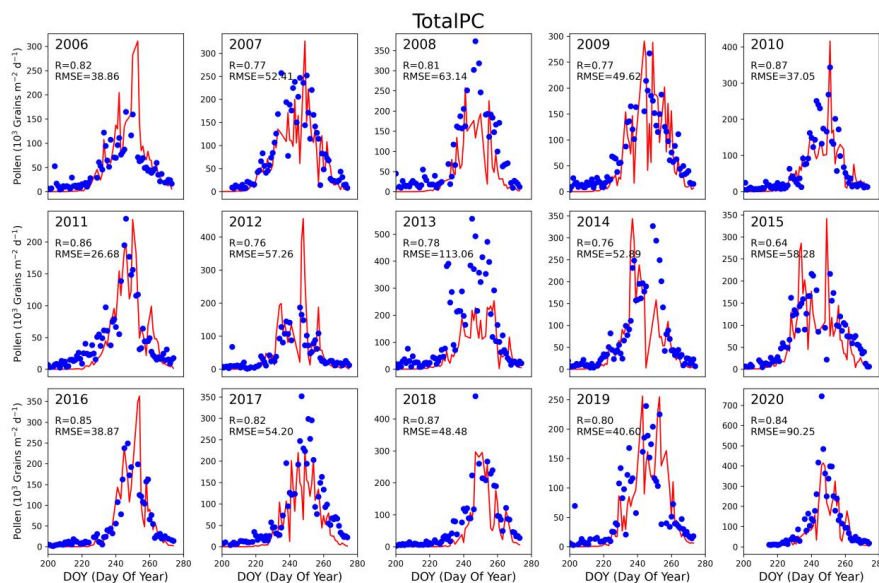
Fig. 17. Time-series distribution of Chenopod under RegCM simulation compared to observations

727

(averaged across effective pollen monitoring sites). The red solid line represents model

728

simulations, while blue dots depict observations



729

730

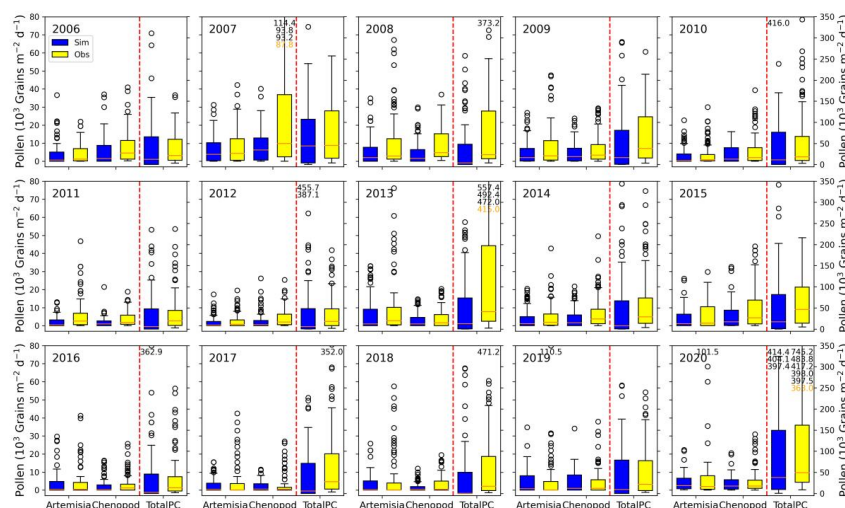
Fig. 18. Time-series distribution of TotalPC under RegCM simulation compared to observations

731

(averaged across effective pollen monitoring sites). The red solid line represents model

732

simulations, while blue dots depict observations



733

734 Fig. 19. Box plot statistics of pollen concentration under RegCM simulation compared to observed
 735 values. Each subplot features box plots denoted by red dashed lines: on the left side, representing
 736 Artemisia and Chenopod concentrations with values referenced on the left y-axis; on the right side,
 737 depicting TotalPC with values referenced on the right y-axis. In each box plot, from bottom to top,
 738 the box and whiskers indicate the minimum, lower quartile, median, upper quartile, and maximum
 739 values (extending up to 1.5 times the interquartile range, IQR). Black circles denote outliers
 740 exceeding 1.5 times IQR. Orange numbers annotated in the subplot indicate the maximum values
 741 unseen within the box, while black numbers denote unseen outliers

742 **4. Conclusion**

743 This study utilized years of autumn pollen concentration data from Beijing,
 744 alongside meteorological and land use data, to develop an autumn pollen emissions
 745 model using autumn phenology and the RF algorithm. We conducted an in-depth
 746 analysis of the spatiotemporal distribution characteristics of Artemisia, Chenopod, and
 747 TotalPC in Beijing and examined their relationships with meteorological factors.
 748 Finally, we validated the accuracy and reliability of the constructed pollen emissions
 749 model using the RegCM. Through a series of simulations and validations, several
 750 significant conclusions and findings were obtained.

751 (1) Construction of the Pollen Emissions Model: By incorporating phenology



752 and the RF algorithm, we calculated autumn pollen emissions, thereby avoiding the
753 poor simulation results of sDOY, eDOY, and annual pollen production based solely on
754 temperature linear simulations. The study demonstrates that using a phenology model
755 for sDOY and eDOY simulations captures the temporal variations of pollen release
756 more accurately, effectively reducing simulation errors. The RF algorithm excels in
757 handling multivariate and nonlinear relationships, significantly improving the
758 simulation accuracy of the pollen emissions model. The optimized annual pollen
759 production simulations better reflect seasonal changes in pollen, showcasing the
760 applicability and reliability of the RF algorithm in processing meteorological and
761 environmental data.

762 (2) Spatiotemporal Distribution Characteristics of Pollen Concentration: The
763 study found significant spatial and temporal variations in pollen concentration in
764 Beijing. The autumn pollen peak occurs between DOY 215-280, with considerable
765 differences in peak times and concentrations among monitoring stations. These
766 differences are closely related to the vegetation types, topographical features, and
767 local climatic conditions around each station. Optimized simulations of pollen
768 concentration data further reveal the spatiotemporal variation patterns of pollen
769 concentrations.

770 (3) Impact of Meteorological Factors on Annual Pollen Emissions:
771 Meteorological factors significantly influence pollen concentrations. The study
772 reveals that temperature, RH, and SSH are crucial factors affecting annual pollen
773 emissions in Beijing. There is a positive correlation between temperature and RH with
774 annual pollen emissions, while SSH has a negative correlation. The response of
775 different pollen types to meteorological factors varies due to their distinct biological
776 characteristics and ecological environments. This comprehensive analysis provides a
777 scientific basis for predicting future changes in pollen concentrations.

778 (4) Validation of Pollen Emissions Models Using the RegCM: The RegCM
779 accurately reflects the daily impact of meteorological factors on pollen emissions.
780 Key physical processes, such as advection, convection, and wet and dry deposition,
781 play essential roles in simulating the atmospheric dispersion and deposition of pollen.



782 This study validated the accuracy and reliability of the optimized emission potential
783 models for three pollen types using RegCM, effectively describing the daily variations
784 in pollen concentrations influenced by meteorological factors and key physical
785 processes. Furthermore, the pollen emissions model developed in this study can be
786 applied to other regions, offering potential for wider application. These
787 comprehensive results provide essential scientific support for pollen monitoring,
788 allergy prevention, and the selection of urban greening plants. Future research can
789 extend these methods and findings to larger-scale pollen emissions simulations and
790 forecasts, enhancing responses to pollen-related public health issues.

791 (5) Limitations and Future Prospects: Despite significant progress in
792 constructing the pollen emissions model and analyzing the spatiotemporal distribution
793 of pollen concentrations, some limitations persist. For broader application, more
794 extensive observation stations are needed to verify the model's accuracy, considering
795 the limited spatiotemporal resolution of current pollen concentration data. Simulating
796 specific species' pollen concentrations requires detailed plant functional type
797 distributions, which significantly impact the spatial distribution of pollen emissions
798 potential. The current research utilizes static plant functional type data, but dynamic
799 data would better reflect the impact of land use changes on pollen climates over
800 various temporal and spatial scales. Additionally, the complex relationship between
801 meteorological factors and pollen concentrations suggests that future research could
802 introduce more environmental and meteorological variables and apply advanced
803 machine learning algorithms to enhance the model's predictive capability.

804 In conclusion, This study successfully constructed a pollen emissions potential
805 model, systematically analyzed the spatiotemporal distribution of different pollen
806 types in autumn in Beijing, and explored their relationship with meteorological factors.
807 The model's accuracy and stability were validated using the RegCM, yielding notable
808 research results. Future research can further validate and extend this approach on a
809 larger scale and with higher resolution, providing comprehensive scientific support
810 for ecological environment protection and public health.



811 **Data availability**

812 Meteorological data were sourced from the China Surface Climate Daily Dataset
813 (<https://data.cma.cn/data/cdcindex/cid/f0fb4b55508804ca.html>), which requires
814 appropriate permissions for access. Pollen data were provided by the Beijing
815 Meteorological Bureau, and the authors do not have permission to share this data.

816 **Authorship contributions**

817 **JL** performed the analysis, investigation, methodology, software development,
818 validation, and original draft preparation. **XA** conceptualized the paper, provided
819 resources, acquired funding, and conducted the review and editing. **ZS** and **CY**
820 contributed resources, visualization, and data curation. **HQ**, **YZ**, and **ZL** were
821 involved in visualization. All authors contributed to manuscript revisions.

822 **Declaration of competing interest**

823 The authors declare that they have no known competing financial interests or personal
824 relationships that could have appeared to influence the work reported in this paper.

825 **Acknowledgments**

826 This work was supported by the National Key Research and Development
827 Program of China (grant number 2022YFC3701205), Science and Technology
828 Development Fund of the Chinese Academy of Meteorological Sciences (grant
829 number 2023Z026) and the National Natural Science Foundation of China (grant
830 number 41975173).

831 **Reference**

- 832 Aerts, R., M. Stas, N. Vanlessen, M. Hendrickx, N. Bruffaerts, L. Hoebeke, N. Dendoncker, S.
833 Dujardin, N. D. Saenen & A. Van Nieuwenhuyse (2020) Residential green space and seasonal
834 distress in a cohort of tree pollen allergy patients. *International Journal of Hygiene and*
835 *Environmental Health*, 223, 71-79.
- 836 Ahmed, A., A. Hakim & A. Becker (2018) Evaluation of eczema, asthma, allergic rhinitis and



- 837 allergies among the Grade-1 children of Iqaluit. *Allergy Asthma Clin. Immunol.* 14, 9.
- 838 Asher, M.I., S. Montefort, B. Björkstén, C.K. Lai, D.P. Strachan, S.K. Weiland & H. Williams
839 (2006) Worldwide time trends in the prevalence of symptoms of asthma, allergic
840 rhinoconjunctivitis, and eczema in childhood: ISAAC Phases One and Three repeat
841 multicountry cross-sectional surveys. *Lancet* 368, 733–743.
- 842 Bai, Y., X. Liu, M. Sun, G. Liu & Y. Meng (2009) Effect of Pollen Pollution on Human Health.
843 *Journal of Anhui Agri. Sci.*, 37(5), 2220-2222. (in Chinese)
- 844 Bastl, K., M. Kmenta, M. Berger & U. Berger (2018) The connection of pollen concentrations and
845 crowd-sourced symptom data: new insights from daily and seasonal symptom load index data
846 from 2013 to 2017 in Vienna. *World Allergy Organization Journal*, 11, 1-8.
- 847 Bishan, C., L. Bing, C. Chixin, S. Junxia, Z. Shulin, L. Cailang, Y. Siqiao & L. Chuanxiu (2020)
848 Relationship between airborne pollen assemblages and major meteorological parameters in
849 Zhanjiang, South China. *PLOS ONE*, 15, e0240160.
- 850 Breiman, L. (2001) Random Forests. *Machine Learning*, 45, 5-32.
- 851 Chen, H., J. Li, L. Cheng, Z. Gao, X. Lin, R. Zhu, L. Yang, A. Tao, H. Hong & W. Tang (2021)
852 China consensus document on allergy diagnostics. *Allergy, Asthma & Immunology Research*,
853 13, 177.
- 854 Chen, J., S. Zhu, P. Wang, Z. Zheng, S. Shi, X. Li, C. Xu, K. Yu, R. Chen, H. Kan, H. Zhang & X.
855 Meng (2024) Predicting particulate matter, nitrogen dioxide, and ozone across Great Britain
856 with high spatiotemporal resolution based on random forest models. *Science of The Total
857 Environment*, 926, 171831.
- 858 Cingi, C., P. Gevaert, R. Mösges, C. Rondon, V. Hox, M. Rudenko, N.B. Muluk, G. Scadding, F.
859 Manole, C. Hupin, W.J. Fokkens, C. Akdis, C. Bachert, P. Demoly, J. Mullol, A. Muraro, N.
860 Papadopoulos, R. Pawankar, P. Rombaux, E. Toskala, L. Kalogjera, E. Prokopakis, P.W.
861 Hellings & J. Bousquet (2017) Multimorbidities of allergic rhinitis in adults: European
862 academy of allergy and clinical immunology task force report. *Clin. Transl. Allergy* 7, 17.
- 863 D'Amato, G., C. Vitale, M. Lanza, A. Molino & M. D'Amato (2016) Climate change, air pollution,
864 and allergic respiratory diseases: an update. *Current opinion in allergy and clinical
865 immunology*, 16, 434-440.
- 866 Damialis, A., C. Fotiou, J. M. Halley & D. Vokou (2011) Effects of environmental factors on



- 867 pollen production in anemophilous woody species. *Trees*, 25, 253-264.
- 868 Emanuel, M.B. (1988) Hay fever, a post industrial revolution epidemic: a history of its growth
869 during the 19th century. *Clin. Allergy* 18, 295–304.
- 870 Frei, T. & E. Gassner (2008) Climate change and its impact on birch pollen quantities and the start
871 of the pollen season an example from Switzerland for the period 1969–2006. *International*
872 *Journal of Biometeorology*, 52, 667-674.
- 873 Gao, Q.Q., Q.Y. Gao, J. Li, F. Shen, S. Ji & L. Guan (2022) Preliminary Study on the Variation
874 Characteristics of Pollen Concentration and Pollen Allergy Grade in Langfang Area in Spring.
875 *Journal of Agricultural Catastrophology*. 12(10): 16-18.(in Chinese)
- 876 Gu, D. & K. Liao (2003) The relationship between urban pollen dispersal and meteorological
877 conditions. *Hubei Meteorology*, (03): 36-37. (in Chinese)
- 878 Guan, L., Q.Y. Gao, H. Li, J. Li & Q.Q. Gao (2021) Characteristics of Airborne Pollen Variation in
879 Langfang City and Its Relationship with Meteorological Factors. *Agricultural technology*
880 *service*. 38(6):93-98.(in Chinese)
- 881 Guzman, A., L. Tonelli, D. Roberts, J. Stiller, M. Jackson, J. Soriano, S. Yousufi, K. Rohan, H.
882 Komarow & T. Postolache. 2007. Mood-worsening with high-pollen-counts and seasonality:
883 a preliminary report. In *Journal of affective disorders*.
- 884 He, H., D. Zhang & B. Qiao (2001) Preliminary approach of the relationship between Airborne
885 pollen amount and meteorological factors in Beijing urban area. *Chin J Microbiol Immunol*.
886 (S2):36-38. (in Chinese)
- 887 He, X., D. Liu, Y. Pan, X. He, M. Zhang & S. Yang (2023) Distribution and sources of fluvial
888 pollen in the middle reaches of the Yellow River in China and their relationship with
889 vegetation and land use. *Science of The Total Environment*, 856, 159109.
- 890 Ibrahim, N.M., F.I. Almarzouqi, F.A. Al Melaih, H. Farouk, M. Alsayed & F.M. AlJassim (2021)
891 Prevalence of asthma and allergies among children in the United Arab Emirates: a
892 cross-sectional study. *World Allergy Organ. J.* 14, 100588.
- 893 Khwarahm, N. R., J. Dash, C. A. Skjøth, R. M. Newnham, B. Adams-Groom, K. Head, E. Caulton
894 & P. M. Atkinson (2017) Mapping the birch and grass pollen seasons in the UK using satellite
895 sensor time-series. *Science of The Total Environment*, 578, 586-600.
- 896 Krishna, M. T., P. A. Mahesh, P. K. Vedanthan, V. Mehta, S. Moitra & D. J. Christopher (2020)



- 897 The burden of allergic diseases in the Indian subcontinent: barriers and challenges. The
898 Lancet Global Health, 8, e478-e479.
- 899 Kurganskiy, A., S. Creer, N. De Vere, G. W. Griffith, N. J. Osborne, B. W. Wheeler, R. N. McInnes,
900 Y. Clewlow, A. Barber & G. L. Brennan (2021) Predicting the severity of the grass pollen
901 season and the effect of climate change in Northwest Europe. Science Advances, 7,
902 eabd7658.
- 903 Lake, I. R., N. R. Jones, M. Agnew, C. M. Goodess, F. Giorgi, L. Hamaoui-Laguel, M. A.
904 Semenov, F. Solomon, J. Storkey & R. Vautard (2017a) Climate change and future pollen
905 allergy in Europe. Environmental health perspectives, 125, 385-391.
- 906 Lei, Y., Y. Miao, Y. Zhao, S. Zhang, H. Cao, X. Lan, Z. Zhang & H. Jin (2023) The effects of
907 meteorological conditions on allergenic airborne pollen in arid Northwest China.
908 Atmospheric Environment, 299, 119647.
- 909 Li, L., D. Hao, X. Li, M. Chen, Y. Zhou, D. Jurgens, G. Asrar & A. Sapkota (2022) Satellite-based
910 phenology products and in-situ pollen dynamics: A comparative assessment. Environmental
911 Research, 204, 111937.
- 912 Li, X., Y. Zhou, L. Meng, G. Asrar, A. Sapkota & F. Coates (2019) Characterizing the relationship
913 between satellite phenology and pollen season: A case study of birch. Remote Sensing of
914 Environment, 222, 267-274.
- 915 Li, Z., Y. Chen, Y. Tao, X. Zhao, D. Wang, T. Wei, Y. Hou & X. Xu (2023) Mapping the personal
916 PM2.5 exposure of China's population using random forest. Science of The Total
917 Environment, 871, 162090.
- 918 Lou, H., S. Ma, Y. Zhao, F. Cao, F. He, Z. Liu, J. Bousquet, C. Wang, L. Zhang & C. Bachert
919 (2017) Sensitization patterns and minimum screening panels for aeroallergens in
920 self-reported allergic rhinitis in China. Scientific reports, 7, 9286.
- 921 Mallo, J., J. Crane, E. von Mutius, J. Odhiambo, U. Keil & A. Stewart (2013) The international
922 study of asthma and allergies in childhood (ISAAC) phase three: a global synthesis. Allergol.
923 Immunopathol. 41, 73-85.
- 924 Meier, M. & C. Bigler (2023) Process-oriented models of autumn leaf phenology: ways to sound
925 calibration and implications of uncertain projections. Geosci. Model Dev., 16, 7171-7201.
- 926 Meng, L., X. Wang, Z. Ouyang, Y. Ren & Q. Wang (2016) Seasonal Dynamics of Airborne Pollens



- 927 and Its Relationship with Meteorological Factors in Beijing Urban Area. *Environmental*
928 *science*, 37 (02): 452-458.(in Chinese)
- 929 Mir, E., C. Panjabi & A. Shah (2012) Impact of allergic rhinitis in school going children. *Asia*
930 *Pacific Allergy*, 2, 93-100.
- 931 Mo, Y., J. Zhang, H. Jiang & Y. H. Fu (2023) A comparative study of 17 phenological models to
932 predict the start of the growing season. *Frontiers in Forests and Global Change*, 5.
- 933 Oleson, K., D. Lawrence, G. Bonan, M. Flanner & E. Kluzek (2010) Technical Description of
934 Version 4.0 of the Community Land Model (CLM), NCAR Technical Note
935 NCAR/TN-478+STR, NCAR, Boulder, USA, 257 pp.
- 936 Qiao, Y., L. Wu, S. Yang, Q. Wang, H. Gu, L. Wei, G. Liu, S. Zhou, P. Wang & M. Song (2023)
937 Metabolomic and transcriptomic analyses provide insights into variations in flavonoids
938 contents between two *Artemisia* cultivars. *BMC Plant Biology*, 23, 288.
- 939 Rahman, A., C. Luo, B. Chen, S. Haberle, M. H. R. Khan, W. Jiang, R. Xiang, J. Liu, L. Wang, G.
940 Lin, M. Yang & V. Thilakanayaka (2020) Regional and seasonal variation of airborne pollen
941 and spores among the cities of South China. *Acta Ecologica Sinica*, 40, 283-295.
- 942 Schmidt, C.W. (2016) Pollen overload: seasonal allergies in a changing climate. *Environ. Health*
943 *Perspect.* 124.
- 944 Septembre-Malaterre, A., M. Lalarizo Rakoto, C. Marodon, Y. Bedoui, J. Nakab, E. Simon, L.
945 Hoarau, S. Savriama, D. Strasberg, P. Guiraud, J. Selambarom & P. Gasque (2020) *Artemisia*
946 *annua*, a Traditional Plant Brought to Light. *International Journal of Molecular Sciences*, 21.
- 947 Sofiev, M., P. Siljamo, H. Ranta & A. Rantio-Lehtimäki (2006) Towards numerical forecasting of
948 long-range air transport of birch pollen: theoretical considerations and a feasibility study.
949 *International Journal of Biometeorology*, 50, 392-402.
- 950 Sofiev, M., P. Siljamo, H. Ranta, T. Linkosalo, S. Jaeger, A. Rasmussen, A. Rantio-Lehtimäki, E.
951 Severova & J. Kukkonen (2013) A numerical model of birch pollen emissions and dispersion
952 in the atmosphere. Description of the emission module. *International Journal of*
953 *Biometeorology*, 57, 45-58.
- 954 Stas, M., R. Aerts, M. Hendrickx, A. Delcloo, N. Dendoncker, S. Dujardin, C. Linard, T. Nawrot,
955 A. Van Nieuwenhuysse & J.-M. Aerts (2021) Exposure to green space and pollen allergy
956 symptom severity: A case-crossover study in Belgium. *Science of The Total Environment*,



- 957 781, 146682.
- 958 Valipour Shokouhi, B., K. de Hoogh, R. Gehrig & M. Eeftens (2024) Estimation of historical daily
959 airborne pollen concentrations across Switzerland using a spatio temporal random forest
960 model. *Science of The Total Environment*, 906, 167286.
- 961 Virro, H., A. Kmoch, M. Vainu & E. Uuemaa (2022) Random forest-based modeling of stream
962 nutrients at national level in a data-scarce region. *Science of The Total Environment*, 840,
963 156613.
- 964 Wang, X. D., M. Zheng, H. Lou, C. Wang, Y. Zhang, M. Bo, S. Ge, N. Zhang, L. Zhang & C.
965 Bachert (2016) An increased prevalence of self-reported allergic rhinitis in major Chinese
966 cities from 2005 to 2011. *Allergy*, 71, 1170-1180.
- 967 Wang, X. Y., T. T. Ma, X. Y. Wang, Y. Zhuang, X. D. Wang, H. Y. Ning, H. Y. Shi, R. L. Yu, D.
968 Yan & H. D. Huang (2018) Prevalence of pollen-induced allergic rhinitis with high pollen
969 exposure in grasslands of northern China. *Allergy*, 73, 1232-1243.
- 970 Wozniak, M. C. & A. L. Steiner (2017) A prognostic pollen emissions model for climate models
971 (PECM1.0). *Geosci. Model Dev.*, 10, 4105-4127.
- 972 Wu, Z., A. Liu, Y. Bai, B. Liu & C. Wang (2011) Study on Evaluation of Economic Benefits from
973 Pollen Forecast and Service in Tianjin. *Meteorological monthly*, 37(5):626-632. (in Chinese)
- 974 Yin, J., F. Yue, L. Wang, H. He, T. Xu, H. Zhang, H. Li, L. Wen, J. Sun & J. Gu (2005) The
975 clinical study of the relationship between allergic rhinitis and allergic asthma in the patients
976 with autumnal pollinosis. *Zhonghua Yi Xue Za Zhi*, 85, 1683-1687.
- 977 Yorimitsu, Y., A. Kadosono, Y. Hatakeyama, T. Yabiku & O. Ueno (2019) Transition from C3 to
978 proto-Kranz to C3-C4 intermediate type in the genus *Chenopodium* (Chenopodiaceae).
979 *Journal of Plant Research*, 132, 839-855.
- 980 Zhang, Y. & A. L. Steiner (2022) Projected climate-driven changes in pollen emissions season
981 length and magnitude over the continental United States. *Nature Communications*, 13, 1234.
- 982 Zhao, Y., Z. Sun, L. Xiang, X. An, X. Hou, J. Shang, L. Han & C. Ye (2023) Effects of pollen
983 concentration on allergic rhinitis in children: A retrospective study from Beijing, a Chinese
984 megacity. *Environmental Research*, 229, 115903.